Open-Gated GaN HEMT-Based pH Detectors Using Patterned Sensing Area

Arathy Varghese, Abdalla Eblabla*, and Khaled Elgaid

***Abstract*—This paper presents a pioneering study on the pH sensing performance of open gated GaN high-electron mobility transistors (HEMTs) with five different device variants, introducing novel approach to patterning the open gate area. The device variants include normal HEMTs with open gate (O-HEMT)-used as reference, with horizontal lines etched in the open gate area (H-HEMTs), with vertical lines etched in the open gate area (V-HEMTs), fully blank etched (B-HEMTs), and with horizontal and vertical lines or grids etched (G-HEMTs). Fabrication of the GaN HEMTs was achieved through Metal Organic Chemical Vapor Deposition (MOCVD), while the source and drain ohmics were fabricated using e-beam evaporation. The sensitivity analysis involved drop casting samples of varying pH onto the open gate area and measuring the device response for acidic (pH=4), basic (pH=10), and neutral (pH=7) solutions. pH values of 4, 7, and 10 for our analysis has been chosen to showcase the sensor's functionality within a range pertinent to common practical applications, such as biological systems and environmental monitoring—environments where these pH levels are typically found. The normalized output drain current has been employed as the sensing metric. Our findings reveal the remarkable novelty of this study, as it demonstrates that G-HEMTs exhibit the highest sensitivity among the variants, with an average sensing current of 1.355 mA/pH. The V-HEMTs displayed a sensitivity of 2.15%, followed by H-HEMTs at 1.98%, and normal HEMTs at 1.16%. Notably, the B-HEMT devices initially showcased good sensitivities; however, their performance declined below that of H-HEMTs beyond 15 V. These results underscore the significance of patterning the open gate area in optimizing the pH sensing capabilities of GaN HEMTs.**

***Index Terms*—AlGaN/GaN HEMT; pH sensor; sensitivity; sensing metric**

I. INTRODUCTION

HIGH-electron mobility transistors (HEMTs) are widely used in a wide variety of applications due to their excellent high-frequency performance, high power density, and low noise characteristics [1]. Gallium nitride (GaN) HEMTs, in particular, have emerged as a promising technology for high-frequency and high-power applications, owing to their high breakdown voltage, high electron mobility, and excellent thermal stability [2, 3]. Recently, there has been growing interest in the use of GaN HEMTs for chemical sensing applications, including pH sensing [4-6]. In pH sensing, GaN HEMTs offer several advantages over conventional sensors, such as direct access to the sensing area, fast response times, and the potential for miniaturization [7, 8]. The pH sensing mechanism in GaN HEMTs is based on the modulation of the surface potential at the open gate area, which is sensitive to the pH of the surrounding solution [9, 10].

pH sensing plays a crucial role in a wide range of applications across various fields. It is vital for environmental monitoring, where pH measurement helps assess water quality and detect pollution in natural water bodies. In biomedical and clinical diagnostics, pH monitoring is essential for studying disease mechanisms, drug interactions, and assessing physiological conditions. pH sensing is also of great importance in agriculture and soil science, aiding in soil analysis and determining optimal pH levels for crop growth. In industrial processes, pH control ensures efficient and consistent operations and adherence to regulatory standards. pH monitoring is critical in aquaculture for maintaining optimal conditions for aquatic organisms, and in the food and beverage industry, it ensures product quality and safety. In summary, pH sensing plays a pivotal role in scientific research, process control, environmental stewardship, and improving human well-being in diverse applications.

Field-Effect Transistors (FETs) have been widely utilized in pH sensing due to their high sensitivity and fast response times [11-13]. However, they typically suffer from poor stability in harsh environments, which limits their long-term reliability. Unlike conventional FETs, GaN HEMTs offer superior chemical and thermal stability due to the robustness of GaN material, making them more suitable for applications in extreme conditions. Moreover, the open-gated GaN HEMT-based sensors in our study show enhanced sensitivity because the two-dimensional electron gas (2DEG) at the AlGaN/GaN interface is directly exposed to the analyte, providing a more immediate and sensitive response to pH changes. This contrasts with traditional FET sensors, where the gate oxide layer can interfere with direct analyte interaction, potentially reducing sensitivity. Diode-based sensors, on the other hand, typically operate by measuring changes in the diode’s forward voltage, which correlates with the concentration of hydrogen ions in the solution [14, 15]. While diode-based sensors are known for their simplicity and low cost, they generally lack the selectivity and sensitivity provided by GaN HEMT sensors. This is partly due to the fact that diodes do not have a gate structure that can be used to modulate the sensitivity and selectivity of the sensor actively.

Further, open gated GaN HEMTs hold significant relevance as

A.Varghese, A. Eblabla, and K. Elgaid are with the School of Engineering, Cardiff University, CF24 3AA.
Corresponding author: A. Eblabla (eblablaa@cardiff.ac.uk).

pH sensors due to several key factors [16]. Firstly, GaN HEMTs offer excellent electrical and chemical properties, making them suitable for pH sensing applications. The high carrier mobility and low noise characteristics of GaN HEMTs enable precise and sensitive measurements of pH changes. Secondly, the open gate structure of GaN HEMTs allows direct exposure of the gate surface to the analyte solution, facilitating rapid and sensitive pH detection. The gate surface serves as the sensing interface, where pH variations induce changes in the surface potential, leading to alterations in the electrical properties of the transistor. This mechanism enables label-free and real-time pH monitoring [17].

This work investigates the relevance of open gated GaN HEMTs as pH sensors by examining the performance of different device variants. The study includes five types of open gate structures: normal open gated HEMTs, H-HEMTs with horizontal lines etched in the open gate area, V-HEMTs with vertical lines etched in the open gate area, B-HEMTs with a fully blank etched gate, and G-HEMTs with both horizontal and vertical lines or grids etched in the gate. All device variants were fabricated together, allowing for direct comparison of their pH sensing performance. Notably, the grid and blank etched devices exhibited similar pH sensitivities, while the unetched open gated device demonstrated the lowest sensitivity. This investigation sheds light on the impact of gate structure patterning on the pH sensing capabilities of open gated GaN HEMTs, providing insights into the design and fabrication of high-performance pH sensors based on this technology.

II. DEVICE FABRICATION

The HEMT epitaxial stacks were grown on a high resistivity Si substrate using Metal Organic Chemical Vapor Deposition (MOCVD).

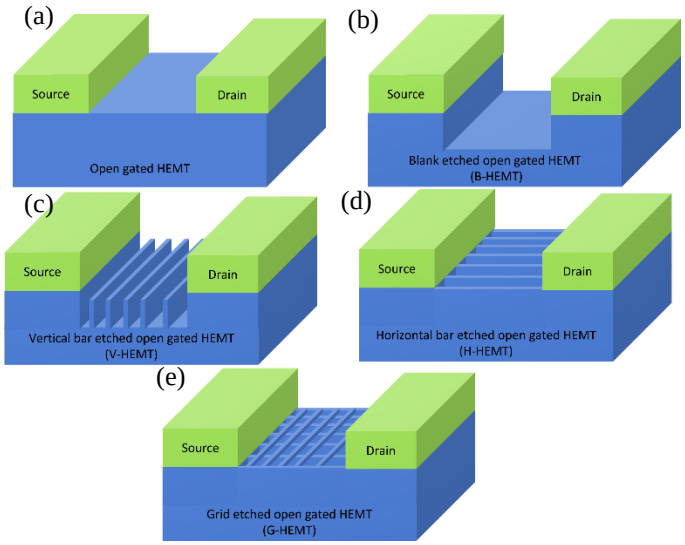

Fig. 1. GaN HEMT pH sensor variants: (a). Open gated traditional HEMT; (b). Completely etched down sensing surface; (c). Vertical bars etched on the sensing area; (d). Horizontal bars etched on the sensing area; (e). Grids etched on the sensing area.

A transition layer with a thickness of 250nm has been used. A thin AlGaN barrier layer of 9 nm was grown on a 1700 nm Fe-doped GaN buffer, with a peak doping concentration of $1 \times 10^{18}/cm^3$, along with a 1 nm AlN spacer. Employing an Fe-doped GaN buffer layer provides numerous advantages over conventional GaN HEMTs with an undoped GaN buffer. These include reduced dislocation density, enhanced carrier mobility, higher thermal conductivity, and controlled threshold voltage, resulting in improved material quality and electrical properties, thereby enhancing overall device power and RF performance [18]. The overall epilayer stacks were capped with a 2 nm GaN, as shown in Fig. 1. The fabrication process followed a standard flow, starting with alignment markers and ohmic metallization. Specifically, a layer sequence of Ti (20 nm), Al (120 nm), Ni (40 nm), and Au (50 nm) was deposited for the source and drain contacts. Mesa isolation was achieved using Cl_2-based inductively coupled plasma-reactive ion etching (ICP-RIE). Surface etching has been done using ICP-RIE based dry etch techniques which will be explained in detail in the following section. The fabricated device variants are shown in Fig. 1. For device passivation, a PECVD-based nitride deposition technique has been employed.

The sensing area in the device is situated within the open gate region, which lies between the source and drain terminals. In order to enhance device performance, novel HEMT variants with patterned structures in this area have been proposed. These patterned variants offer improved sensitivities by increasing the sensing area and bringing it into closer proximity with the 2DEG (Two-Dimensional Electron Gas) channel, in comparison to the conventional open gated device. To validate the performance enhancement, a comparison has been conducted between the proposed patterned HEMT variants and the traditional open gated HEMT. This comparative analysis serves to confirm the superior performance of the patterned variants in terms of enhanced sensitivities. By strategically modifying the structure within the open gate area, these patterned HEMT variants unlock the potential for improved sensing capabilities, further advancing the field of HEMT-based sensors.

II. ETCHING AND SURFACE MORPHOLOGY

The surface etching process commenced by applying a positive photoresist (S1813) to the samples, creating patterned layers with a thickness of around 1.3 µm. This photoresist served as a flexible etch mask, offering improved process flexibility with simpler and cost-effective processing steps that could be easily integrated into the main process line. To enhance adhesion, the patterned photoresist underwent a post-baking procedure at 95°C for 30 minutes. Subsequently, these patterned samples

were placed on a 4-inch silicon carrier wafer to facilitate cooling during the etching process. The sample temperature was maintained at 25°C using a chiller. The patterned samples were then simultaneously processed and etched in the Oxford Instruments PlasmaPro System 100 Cobra ICP etching system, which allowed for accurate comparative analysis. The etcher's plasma was inductively coupled through a 13.56 MHz coil, with independent control over energy provided by 13.56 MHz RF biasing applied to the substrate. The etching chemistry involved a mixture of BCl_3 and Cl_2, delivered through mass flow-controlled process gas lines. Prior to initiating the etch process, the chamber was evacuated to a base pressure of approximately 2×10^{-5} mTorr. The etch gases were introduced into the chamber through an annular region located on the side of the chamber lid. The process utilized an ICP power of 700 W, an RIE power of 60 W, and a pressure of 50 mTorr. The etch rate and depth were assessed using a surface profilometer, which revealed an achieved etch depth and etch rate of approximately 8 nm and 52 nm/min, respectively. The resulting etched mesa profile and surface morphology were examined using scanning electron microscopy (SEM), as shown in Fig. 2.

III. HEMT AS pH SENSOR

Noteworthy findings have emerged in the field of gateless HEMT sensors, where high sensitivity to electrolyte solutions has been reported [19]. The response to pH has been effectively modeled by quantifying the voltage change resulting from alterations in surface charge, induced by the formation of pH-dependent hydroxyl groups. This modeling approach provides valuable insights into the relationship between pH variations and voltage response, facilitating a deeper understanding of pH-dependent phenomena and enabling the development of precise pH sensing technologies. An advantageous aspect of the proposed pH sensing approach is that the output drain current can be utilized as a reliable sensing metric. In the experimental setup, less than 1 µl of the pH solution was carefully deposited between the source and drain using a micropipette, with the process closely monitored under an imaging microscope to prevent short-circuiting. This precision ensured the isolation of the contacts during pH sensing measurements. By monitoring the variations in the output drain current, it becomes possible to accurately assess changes in pH levels [20, 9]. This offers a convenient and effective means of quantifying pH values, allowing for precise and real-time pH sensing capabilities. The output current I_{DS} in the device is expressed as:

$$I_{DS} = \frac{q \in AlGaN}{d}\left(V_{Gs} - \left(\emptyset_s + E_F - \left(\Delta E_C AlGaN + \frac{q^2}{\in AlGaN}{\sigma_{AlN}}^2 t_{AlN} + V(x)\right) * \frac{V_s E(x)}{\sqrt{E^2(x) + (\frac{V_{Sat}}{\mu})^2}}\right.\right. \quad (1)$$

Where, q represents the charge of an electron, $\in AlGaN$ denotes the effective permittivity of AlGaN, σ_{AlN} represents the polarization density in the spacer AlN layer, t_{AlN} is 1 nm $\Delta E_C AlGaN$ represents the effective conduction band offset resulting from the hetero interface due to the AlGaN layer [9]. Furthermore, $V(x)$ denotes the channel potential in the two-dimensional electron gas (2DEG) along the x-axis, V_{Sat} represents the saturation velocity, $E(x)$ signifies the electric field intensity, μ denotes the low-field mobility, and d refers to the effective distance between the gate and the 2DEG channel, as determined by the expression:

$$d = t_{spacer} + t_{barrier} + \Delta d_{2DEG} \quad (2)$$

Where $t_{spacer} = t_{AlN} = 1\ nm$, $t_{barrier} = 9\ nm$, and Δd_{2DEG} is the separation of 2DEG from the AlN/GaN interface. When a pH solution is applied to the device, it transitions from open gated HEMT to a solution gated HEMT configuration. The schematic diagram of HEMT being used in pH sensing is shown in Fig. 3. In this state, the pH solution serves as the gate, altering the device's electrical properties in response to the pH level of the solution. This transition enables the device to function as a pH sensor, detecting and analyzing pH changes in real-time.

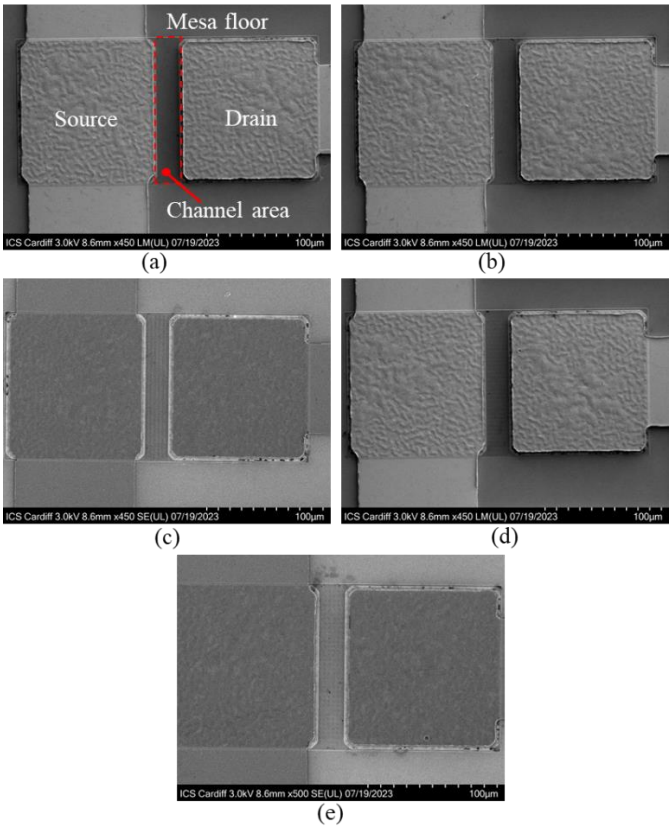

Fig. 2. SEM images of the fabricated GaN HEMT pH sensors: (a). Open gated traditional HEMT; (b). Completely etched down sensing surface; (c). Vertical bars etched on the sensing area; (d). Horizontal bars etched on the sensing area; (e). Grids etched on the sensing area.

The effective gate bias due to the solution gate can be expressed as [21]:

$$V_{sol\_gate} = Q_{pH} * {}^{E}/_{Q} \quad (3)$$

Where, Q_{pH} is the volume charge density per m3 within the pH solution in coulombs. The pH sensing characteristics have

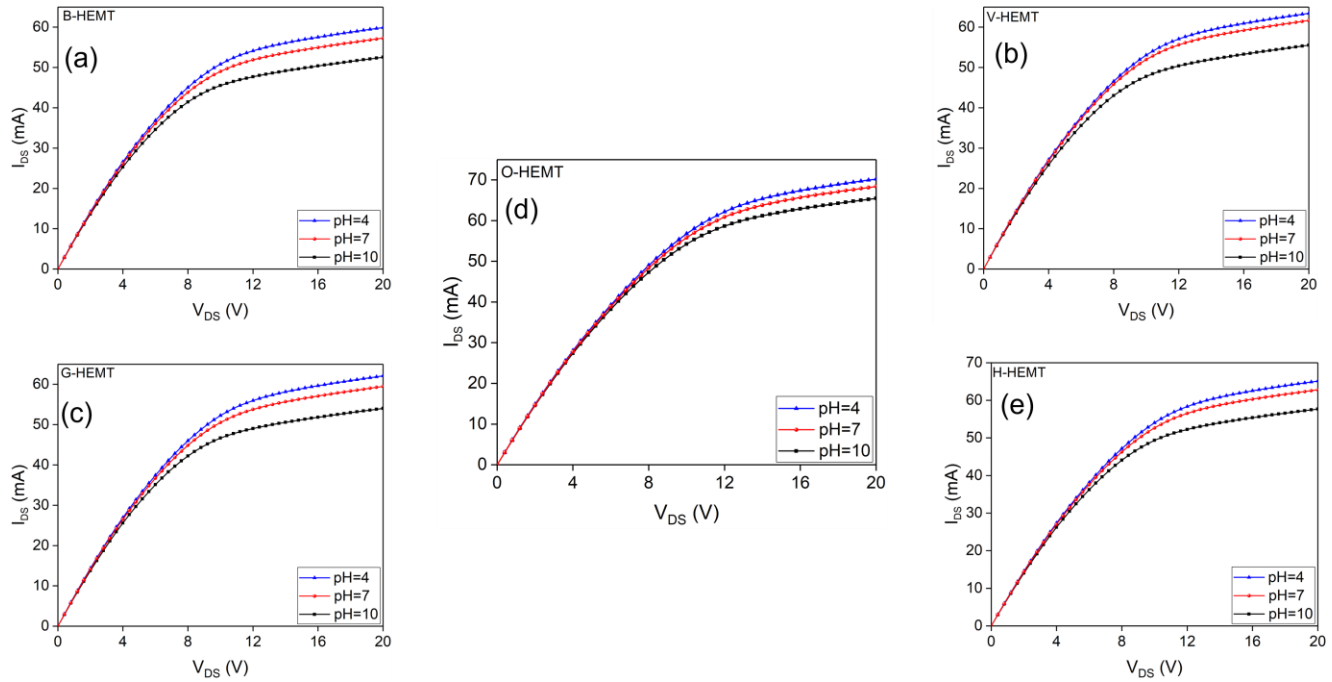

Fig. 5. I_{DS} variation on dispensing pH solution-(a). B-HEMT, (b). V-HEMT, (c). G-HEMT, (d). O-HEMT, and (e). H-HEMT.

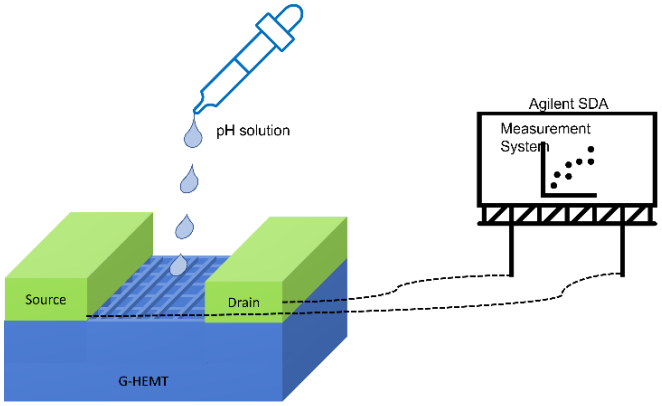

Fig. 3. pH solution being dropped on the open gate area of GaN HEMT.

been measured using DC measurements with an Agilent Semiconductor device analyzer. The variation in drain current has been used as sensing metric for sensitivity analysis.

$$\Delta I_{Davg} = \frac{\frac{abs(\Delta I_{D(pH=4)})}{3} + \frac{abs(\Delta I_{D(pH=10)})}{3}}{2} \quad (4)$$

The average sensing current in the device ΔI_{Davg} is the average of current variations (ΔI_D) for solutions of pH 4, and 10. The drain current at pH=7 is considered as reference for sensitivity analysis [21].

$$\Delta I_{DS} = abs\left(I_{DS\,(pH=x)} - I_{DS\,(pH=7)}\right) \quad (5)$$

The device sensitivity S can be expressed as

$$S = {}^{\Delta I_{DS}}/_{I_{DS}} \times 100\% \quad (6)$$

IV. RESULTS AND DISCUSSION

Sensitivity analysis has been conducted using three different pH samples, representing the acidic, neutral, and alkaline ranges.

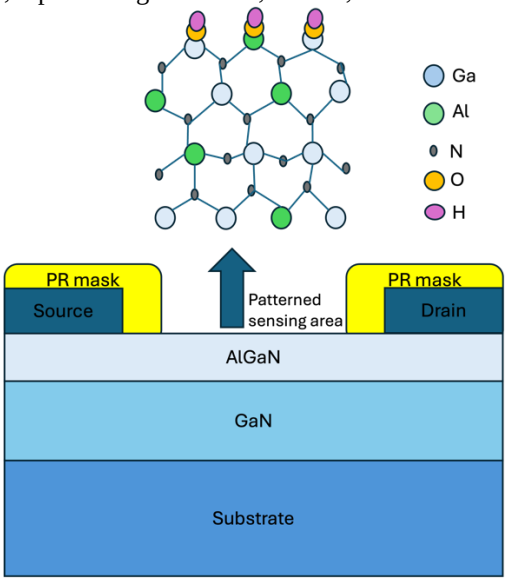

Fig. 4. Sensing mechanism and PR encapsulation to isolate source and drain.

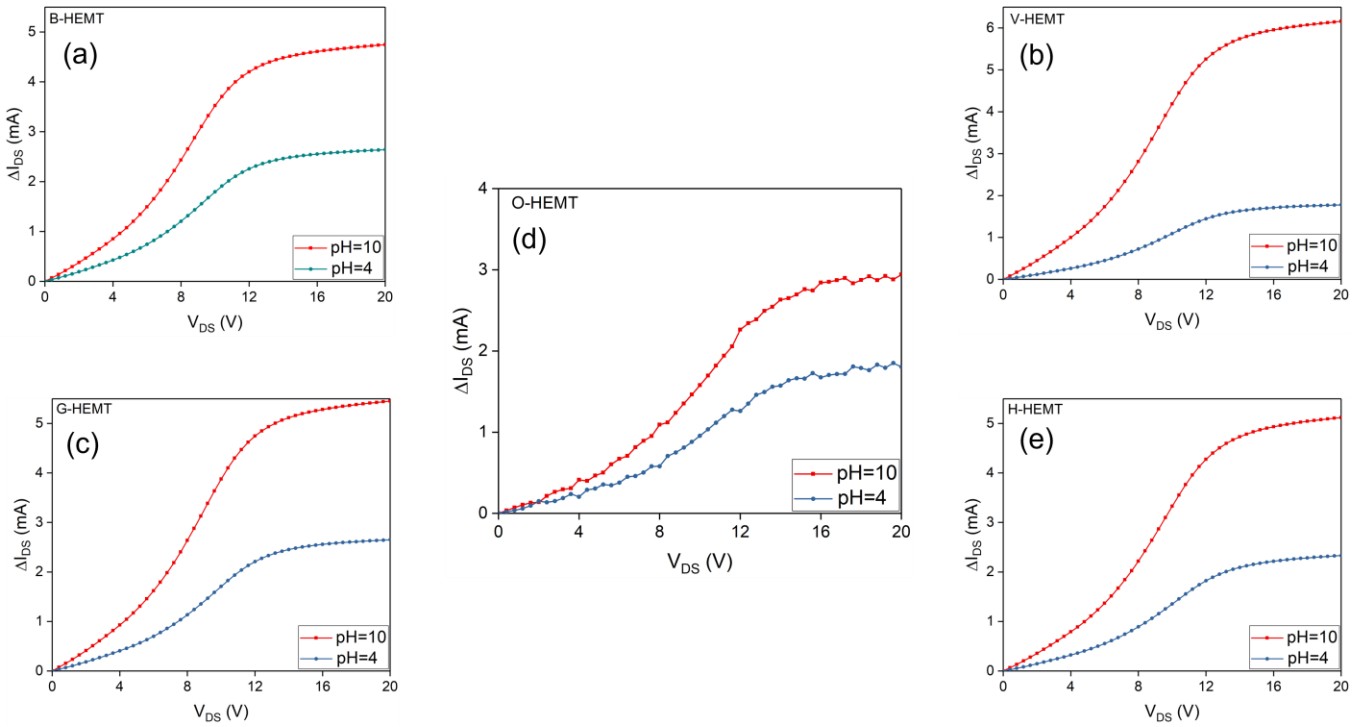

Fig. 6. Sensing currents -(a). B-HEMT, (b). V-HEMT, (c). G-HEMT, (d). O-HEMT, and (e). H-HEMT.

The pH solution has been dropped on the gate of the device using a micropipette capable of dispensing 1 µl of solution. The schematic representation of the pH sensing mechanism in the patterned open-gated AlGaN/GaN HEMT, which includes the thick 5.5 um AZ4562 photoresist encapsulation to isolate the source and drain regions from short-circuiting during drop casting, is presented in Fig. 4. When an acidic solution has been introduced, the quantum well at the hetero interface has deepened, while it has become shallower with the introduction of a basic solution [8, 9, 22]. The depth of the quantum well at the AlGaN/GaN interface is modulated by the surface potential, which is affected by the adsorption of H+ and OH- ions. In an acidic environment, the increase in H+ ion concentration leads to an increase in surface potential, thereby deepening the quantum well, which, in turn, increases the carrier density in the two-dimensional electron gas (2DEG). Conversely, a basic environment introduces more OH- ions, decreasing the surface potential and making the quantum well shallower, reducing the carrier density. These modulations in carrier density directly influence the device's current density and output current.

This change in channel potential results in varying device current density and output current. Figure 5 (a-e) illustrates the drop in output currents with pH solutions. Traditional open gated HEMTs exhibit minimal variation, while increasing alkalinity shows higher current variations ΔI_{DS}, indicating the greater influence of negative charges on the channel's 2DEG compared to positive surface charge. These current variations are presented in Figure 6 (a-e).

Table I
DEVICE SENSITIVITIES

Device	B-HEMT	V-HEMT	G-HEMT	O-HEMT	H-HEMT
S	1.808 %	1.693 %	1.842 %	0.756 %	1.482 %

pH sensing was consistently performed for durations ranging from a few seconds to two minutes, resulting in stable sensor signals. Repeated measurements were taken at least three times for each device variant, showing negligible variation and indicating the reproducibility and reliability of the sensor responses. The results obtained from our experimental analysis reveal significant advancements in the sensing capabilities of H-HEMTs compared to the conventional open gated HEMTs. Specifically, the average sensing current in H-HEMTs exhibits a remarkable 84% increase, demonstrating the enhanced performance of this design. Furthermore, our investigation extends to other etched HEMTs, which display even greater than 100% increase in sensing currents, highlighting the effectiveness of these modified structures in achieving superior sensing capabilities. These findings hold great promise for a wide range of applications, particularly in critical areas such as biomedical and environmental sensing, where the devices' excellent sensitivities and high-resolution output can contribute to precise and reliable data acquisition. The average sensing currents and device sensitivities are shown in Fig. 7 and Fig. 8 respectively.

The improved sensitivity observed after etching can be attributed to the proximity of the sensing area to the 2DEG

channel in the B-HEMTs. Comparative analysis shown in Table I reveals that the blank etched B-HEMT exhibits the highest sensitivity of 1.808%, surpassing the sensitivities of the H-HEMTs (1.482%) and V-HEMTs (1.693%). These results suggest that the absence of etched patterns on the surface provides superior sensitivity compared to the minor pattern etching. However, the G-HEMTs display the highest pH sensitivity of 1.842%. This enhanced sensitivity is attributed to the increased surface area resulting from the etched grid pattern, along with the proximity of the sensing grid's bottom area to the 2DEG channel.

The introduction of horizontal and vertical etchings in the open gate area, as seen in H-HEMTs and V-HEMTs, modifies the surface area that interacts with H+ and OH- ions, affecting the 2DEG density and, subsequently, the device sensitivity to pH changes. The G-HEMTs, with grid patterns etched into the gate, combine the effects of both horizontal and vertical lines, which was hypothesized to enhance the sensitivity further. Interestingly, the B-HEMTs, with a fully blank etched gate, presented a similar sensitivity to the G-HEMTs, indicating that the increased edge area available for protonation and deprotonation is not the sole factor contributing to sensitivity. The comparison highlights the impact of different etching patterns on the sensitivity of the GaN HEMTs, emphasizing the potential for optimizing sensor performance through strategic design choices.

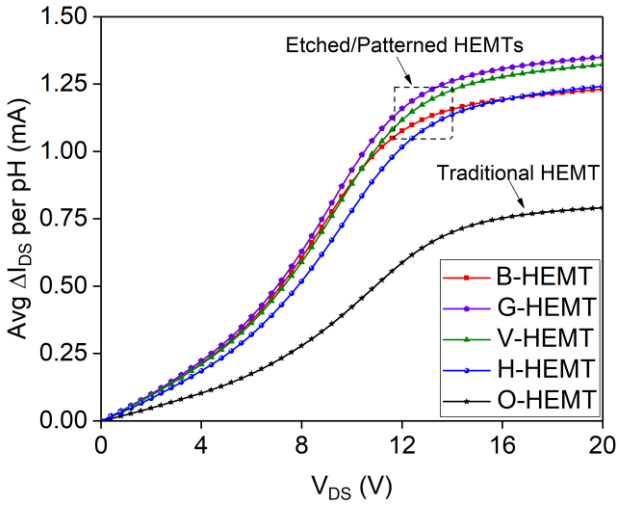

Fig. 7. Average sensing currents-comparative analysis.

V. COMPARATIVE ANALYSIS

G-HEMT sensor presented in this work showcases an average sensing current of 1.355 mA/pH, which indicates a significant advance over several previously reported HEMT-based pH sensors. The analysis considers the sensing current as a key performance indicator, as it directly reflects the device's ability to transduce pH changes into electrical signals.

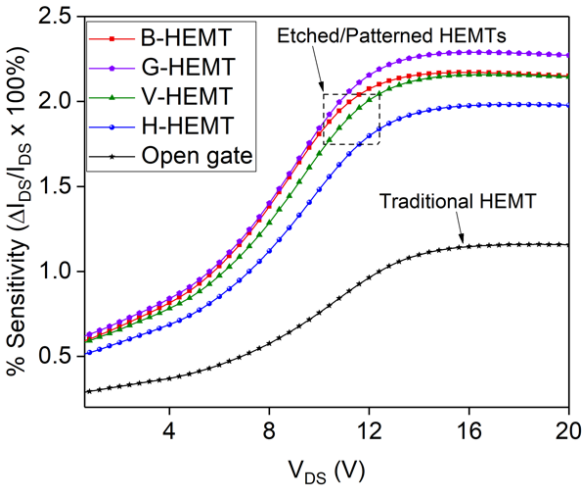

Fig. 8. Device sensitivity.

Table II
COMPARISON OF SENSING CURRENT PERFORMANCE IN GaN HEMT-BASED pH SENSORS

Study	Year	Sensing Parameter	Value
Kang et al. [17]	2007	Sensing Current (µA/pH)	37
Yan Dong et al. [26]	2018	Sensing Current (mA/pH)	1.35
Dong et al. [7]	2018	Sensing Current (µA/pH)	4.6
Sharma et al. [25]	2020	Sensing Current (µA/mm/pH)	4.32
Liu et al. [26]	2023	Sensing Current (µA/pH)	285.7
This work (G-HEMT)	2024	Sensing Current (mA/pH)	1.355

Table II provides a concise comparison of the sensing current values from various studies. As illustrated in the table, our G-HEMT sensors not only improve upon the sensing current observed in some earlier studies but also demonstrate the effectiveness of our novel etching patterns in enhancing sensitivity. For instance, the sensors reported by Dong et al. and Sharma et al. show sensing currents in the microampere range per pH unit, highlighting the considerable increase in our sensors' output [24, 25].

The AlGaN/GaN heterostructure pH sensor with multi-sensing segments developed by Dong et al. reported a close sensitivity of 1.35 mA/pH, similar to our findings. However, our design introduces a nuanced approach to the etching pattern that augments the surface-area-to-volume ratio, thereby providing heightened sensitivity and a more refined response to pH variations [7].

Liu et al. (2023) demonstrated a significant improvement in sensing current with their novel application of visible light communication technology, achieving 285.7 µA/pH. This underscores the rapid progress in HEMT sensor technology and

the potential for diverse applications. Despite the impressive sensing current, our G-HEMT sensors prioritize a balance between high sensitivity and practicality for broader application scenarios [26]. Through this analysis, it becomes evident that the innovative architectural modifications in GaN HEMT-based sensors, as employed in our study, serve as pivotal steps towards achieving high precision and responsiveness in pH sensing, essential for biological and environmental monitoring applications.

VI. CONCLUSION

Our investigation into the sensitivity of GaN HEMTs with different etching patterns has provided valuable insights into their performance characteristics. The results demonstrate that etching plays a crucial role in enhancing the sensitivity of the devices. Among the tested variants, the blank etched B-HEMT exhibited the highest sensitivity of 1.808%, outperforming the H-HEMTs (1.482%) and V-HEMTs (1.693%). This finding emphasizes the significance of the absence of etched patterns on the surface for achieving superior sensitivity. However, it is worth noting that the G-HEMTs, with their etched grid pattern, showcased the highest pH sensitivity of 1.842%. This enhanced sensitivity can be attributed to the increased surface area and the proximity of the sensing grid to the 2DEG channel. Overall, our study highlights the importance of optimizing the etching pattern in GaN HEMTs to achieve optimal sensing capabilities. The results provide valuable guidance for the design and fabrication of high-performance pH sensors. By carefully selecting the etching pattern, researchers can tailor the sensitivity of the sensors to meet specific application requirements. These findings contribute to the advancement of GaN HEMT-based pH sensing technology and pave the way for the development of more efficient and reliable biosensors in various fields, including biomedical and environmental applications.

ACKNOWLEDGMENT

This work was supported by the Engineering and Physical Sciences Research Council (EPSRC) M-Hub under Grant EP/P006973/1.

REFERENCES

[1] J. U. Duncombe, “Infrared navigation—Part I: An assessment of feasibility,” *IEEE Trans. Electron Devices*, vol. ED-11, no. 1, pp. 34–39, Jan. 1959, doi: 10.1109/TED.2016.2628402.

[2] E. P. Wigner, “Theory of traveling-wave optical laser,” *Phys. Rev*., vol. 134, pp. A635–A646, Dec. 1965.

[3] P. Kopyt *et al., “*Electric properties of graphene-based conductive layers from DC up to terahertz range,” *IEEE THz Sci. Technol.,* to be published, doi: 10.1109/TTHZ.2016.2544142. *(Note: If a paper is still to be published, but is available in early access, please follow ref [5]).)*

[4] R. Fardel, M. Nagel, F. Nuesch, T. Lippert, and A. Wokaun, “Fabrication of organic light emitting diode pixels by laser-assisted forward transfer,” *Appl. Phys. Lett.*, vol. 91, no. 6, Aug. 2007, Art. no. 061103.

[5] D. Comite and N. Pierdicca, "Decorrelation of the near-specular land scattering in bistatic radar systems," *IEEE Trans. Geosci. Remote Sens.*, early access, doi: 10.1109/TGRS.2021.3072864. (*Note: This format is used for articles in early access. The doi must be included.)*

[6] H. V. Habi and H. Messer, "Recurrent neural network for rain estimation using commercial microwave links," *IEEE Trans. Geosci. Remote Sens.*, vol. 59, no. 5, pp. 3672-3681, May 2021. [Online]. Available: https://ieeexplore.ieee.org/document/9153027.

[7] Dong, Y., Son, D.H., Dai, Q., Lee, J.H., Won, C.H., Kim, J.G., Kang, S.H., Lee, J.H., Chen, D., Lu, H. and Zhang, R., 2018. AlGaN/GaN heterostructure pH sensor with multi-sensing segments. *Sensors and Actuators B: Chemical*, *260*, pp.134-139.

[8] Bhat, A.M., Shafi, N., Sahu, C. and Periasamy, C., 2021. AlGaN/GaN HEMT pH sensor simulation model and its maximum transconductance considerations for improved sensitivity. *IEEE Sensors Journal*, *21*(18), pp.19753-19761.

[9] A. Varghese, C. Periasamy, L. Bhargava, S. B. Dolmanan and S. Tripathy, "Linear and Circular AlGaN/AlN/GaN MOS-HEMT-based pH Sensor on Si Substrate: A Comparative Analysis," in *IEEE Sensors Letters*, vol. 3, no. 4, pp. 1-4, April 2019, Art no. 4500404, doi: 10.1109/LSENS.2019.2909291.

[10] Pyo, J.Y., Jeon, J.H., Koh, Y., Cho, C.Y., Park, H.H., Park, K.H., Lee, S.W. and Cho, W.J., 2018. AlGaN/GaN high-electron-mobility transistor pH sensor with extended gate platform. *AIP Advances*, *8*(8), p.085106.

[11] Ren, H., Liang, K., Li, D., Chen, Y., Tang, Y., Wang, Y., Li, F., Liu, G. and Zhu, B., 2023. Field-effect transistor-based biosensor for pH sensing and mapping. *Advanced Sensor Research*, *2*(8), p.2200098.

[12] Wang, Y., Yang, M. and Wu, C., 2020. Design and implementation of a pH sensor for micro solution based on nanostructured ion-sensitive field-effect transistor. *Sensors*, *20*(23), p.6921.

[13] Wang, K., Liu, X., Zhao, Z., Li, L., Tong, J., Shang, Q., Liu, Y. and Zhang, Z., 2023. Carbon nanotube field-effect transistor based pH sensors. *Carbon*, *205*, pp.540-545.

[14] Orpen, D., Beirne, S., Fay, C., Lau, K.T., Corcoran, B. and Diamond, D., 2011. The optimisation of a paired emitter–detector diode optical pH sensing device. *Sensors and Actuators B: Chemical*, *153*(1), pp.182-187.

[15] Mohammadi, E. and Manavizadeh, N., 2018. Performance evaluation of innovative ion-sensitive field effect diode for pH sensing. *IEEE Sensors Journal*, *19*(4), pp.1239-1244.

[16] Yang, X., Ao, J., Wu, S., Ma, S., Li, X., Hu, L., Liu, W. and Han, C., 2020. Low-power pH sensor based on narrow channel open-gated Al0. 25Ga0. 75N/GaN HEMT and package integrated polydimethylsiloxane microchannels. *Materials*, *13*(22), p.5282.

[17] Kang, B.S., Wang, H.T., Ren, F., Gila, B.P., Abernathy, C.R., Pearton, S.J., Johnson, J.W., Rajagopal, P., Roberts, J.C., Piner, E.L. and Linthicum, K.J., 2007. pH sensor using AlGaN⁄GaN high electron mobility transistors with Sc2O3 in the gate region. Applied physics letters, 91(1)

[18] Hou-Yu-Wang, Kai-Di-Mai, L. -Y. Peng, Y. -H. Cheng and H. -C. Chiu, "Effects of the Fe-doped GaN buffer in AlGaN/GaN HEMTs on SiC substrate," *2015 IEEE International Conference on Electron Devices and Solid-State Circuits (EDSSC)*, Singapore, 2015, pp. 645-648, doi: 10.1109/EDSSC.2015.7285198.

[19] G. Steinhoff, M. Hermann, W. J. Schaff, L. F. Eastman, M. Stutzmann, and M. Eickhoff, “p H response of GaN surfaces and its application for p H-sensitive field-effect transistors,” *Appl. Phys. Lett.*, vol. 83, no. 1, pp.177-179.

[20] Xue, D., Zhang, H., ul Ahmad, A., Liang, H., Liu, J., Xia, X., Guo, W., Huang, H. and Xu, N., 2020. Enhancing the sensitivity of the reference electrode free AlGaN/GaN HEMT based pH sensors by controlling the threshold voltage. *Sensors and Actuators B: Chemical*, *306*, p.127609.

[21] Varghese, A., Periasamy, C. and Bhargava, L., 2018. Analytical modeling and simulation-based investigation of AlGaN/AlN/GaN Bio-HEMT sensor for C-erbB-2 detection. *IEEE Sensors Journal*, *18*(23), pp.9595-9603.

[22] Varghese, A., Periasamy, C., Bhargava, L., Dolmanan, S.B. and Tripathy, S., 2020. Fabrication and modeling-based performance analysis of circular GaN MOSHEMT-based electrochemical sensors. *IEEE Sensors Journal*, *21*(4), pp.4216-4224.

[23]Varghese, A., Chinnamuthan, P. and Bhargava, L., 2020. Fabrication and pH-sensitivity analysis of MOS-HEMT dimensional variants for bio-sensing applications. *IEEE Transactions on NanoBioscience*, *20*(1), pp.28-34.

[24] Dong, Y., Son, D.H., Dai, Q., Lee, J.H., Won, C.H., Kim, J.G., Chen, D., Lee, J.H., Lu, H., Zhang, R., et al., 2018. "High Sensitive pH Sensor Based on AlInN/GaN Heterostructure Transistor." *Sensors*, vol. 18, no. 1314.

[25] Sharma, N., Mishra, S., Singh, K., Chaturvedi, N., Chauhan, A., Periasamy, C., Kharbanda, D.K., Parjapat, P., Khanna, P.K. and

Chaturvedi, N., 2019. High-resolution AlGaN/GaN HEMT-based electrochemical sensor for biomedical applications. *IEEE Transactions on Electron Devices*, *67*(1), pp.289-295.

[26] Liu, L., Zhang, H., Xu, R., Zhong, G., Huang, H., Guo, W., Xu, N. and Liang, H., 2022. Novel AlGaN/GaN HEMT pH Sensor for Real-Time Monitoring Based on Visible Light Communication Technology. *IEEE Electron Device Letters*, *44*(1), pp.120-123.